Palaeogeography, Palaeoclimatology, Palaeoecology 510 (2018) 40–48

Contents lists available at ScienceDirect

Palaeogeography, Palaeoclimatology, Palaeoecology

journal homepage: www.elsevier.com/locate/palaeo

Distinct responses of East Asian and Indian summer monsoons to astronomical insolation during Marine Isotope Stages 5c and 5e

Zhengguo Shi[a,b,*], Yanjun Cai[a], Xiaodong Liu[a,b], Yingying Sha[a]

[a] State Key Laboratory of Loess and Quaternary Geology, Institute of Earth Environment, Chinese Academy of Sciences, Xi'an 710061, China
[b] CAS Center for Excellence in Tibetan Plateau Earth Sciences, Beijing 100101, China

ARTICLE INFO

Keywords:
Asian monsoon
Numerical experiment
Climate sensitivity
Stalagmite $\delta^{18}O$
Moisture

ABSTRACT

Loess and stalagmite records in China show different responses of Asian monsoon to the astronomical insolation during Marine Isotope Stage (MIS) 5c and 5e, raising the question whether the amplitudes of the whole Asian monsoon are linearly controlled by the astronomical summer insolation changes and whether the regional differences exist. In this study, a set of numerical experiments are conducted for these stages to examine the sensitivity of Asian summer monsoon to changes in the astronomical parameters. The results highlight a complicated response changing with regions and signals. The East Asian monsoon is remarkably stronger during MIS-5e, which is characterized by southerly winds, primarily due to the anomalous anticyclone over northwestern Pacific. The intensified East Asian monsoon leads to less precipitation in the eastern China and Japan but more in the further north and northwest. However, the Indian monsoon circulation does not vary significantly while the precipitation over Arabian Sea is significantly promoted by the upward air motion. Change in water vapor sources of Indian and Pacific Oceans qualitatively explains the observed differences in stalagmite $\delta^{18}O$ records, implying that these proxy changes are primarily controlled by the water vapor delivery from oceans, at least on the astronomical timescale.

1. Introduction

The dominant role of astronomical insolation in controlling the Asian monsoon variation is proposed decades before (Kutzbach, 1981) and this hypothesis has then been intensively supported by various geological records and model simulations (Liu et al., 2003; Kutzbach et al., 2008; Wang et al., 2008; Liu and Shi, 2009; Shi et al., 2011; Li et al., 2013; Yin et al., 2014; Caley et al., 2014; Sun et al., 2015; Cheng et al., 2016). Among studies, the amplitude of Asian summer monsoon is usually considered as a linear response to the astronomical insolation, i.e., the larger insolation is the stronger Asian monsoon is, because large insolation reaching the earth traditionally induces remarkable land-ocean thermal contrast at surface.

One surprising example is the inconsistency between the reconstructed Asian monsoon intensities during Marine Isotope Stage (MIS) 5 from the loess and cave stalagmites collected in China (Fig. 1); in two sub-stages 5c and 5e which correspond to two peaks of northern summer insolation, the responses of Asian monsoon deduced from different records exert distinct amplitudes (Rao et al., 2014). In MIS-5e with larger Milankovitch forcing at 65°N than MIS-5c, the summer monsoon intensity indicated by the magnetic susceptibility of loess and some cave $\delta^{18}O$ is stronger (Kelly et al., 2006; Sun et al., 2006; Cai et al., 2010, 2015; Sun et al., 2015); but a weaker signal is found both for monsoonal and inland areas in other records in this stage (Wang et al., 2008; Cheng et al., 2012). Thus, this raises the question whether or not the long-thought linear response of Asian monsoon to the astronomical forcing (Kutzbach, 1981) is true, especially for the northern insolation peaks. Although the insolation differences are more complicated because they do not be vary consistently among latitudes, these responses of monsoon at insolation peaks, such as MIS-5c and MIS-5e, are still worthy of being evaluated to examine the potential spatial features.

Compared to magnetic susceptibility of the loess, which is a traditional indicator of East Asian summer monsoon (e.g., An et al., 1991; Sun et al., 2006), the proxy significance of cave $\delta^{18}O$ in southern China receives certain suspicion recently (Clemens et al., 2010; Rao et al., 2016; Liu et al., 2017). Some people have argued that the $\delta^{18}O$ records do represent the intensity of the East Asian monsoon precipitation, which strongly correlates to the southerly monsoon winds (Liu et al., 2014); but others believed that it is not principally influenced by the local monsoon but more likely by the Indian monsoon (Pausata et al., 2011). Considering this, two candidate answers for the above-mentioned

* Corresponding author at: State Key Laboratory of Loess and Quaternary Geology, Institute of Earth Environment, Chinese Academy of Sciences, Xi'an 710061, China.
E-mail address: shizg@ieecas.cn (Z. Shi).

https://doi.org/10.1016/j.palaeo.2017.12.029
Received 26 May 2017; Received in revised form 25 December 2017; Accepted 25 December 2017
Available online 29 December 2017
0031-0182/

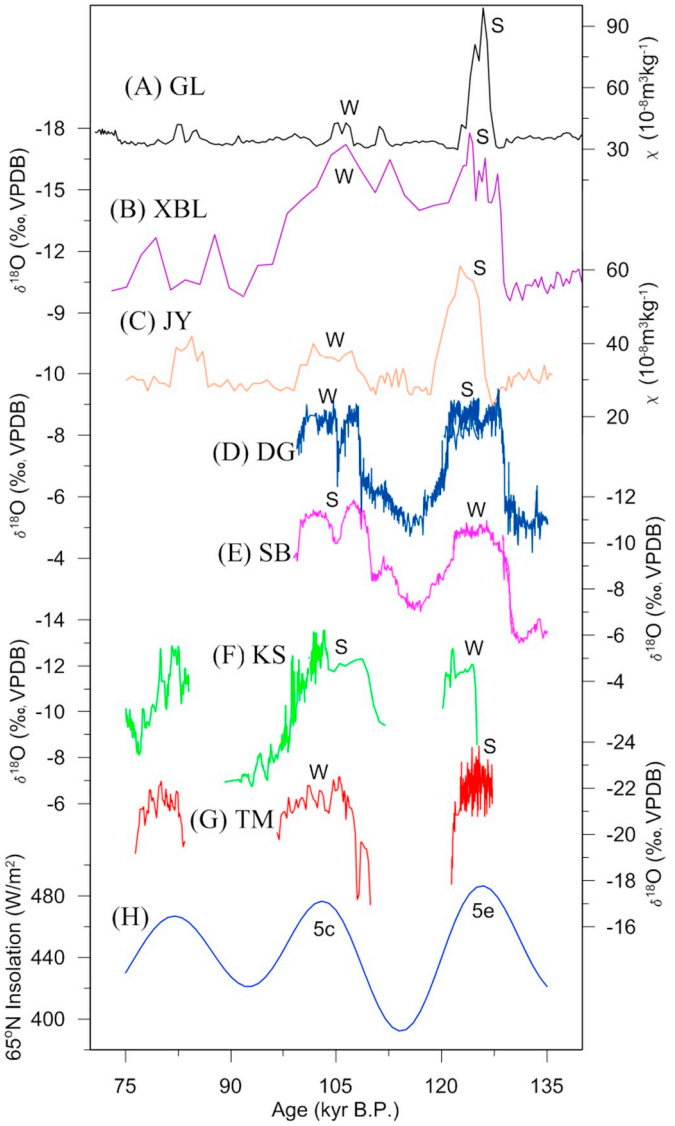

Fig. 1. Different amplitude responses of Asian monsoon proxies during MIS-5c and MIS-5e: (A) Gulang loess magnetic susceptibility (black) (Sun et al., 2015); (B) Xiaobailong cave $\delta^{18}O$ (purple) (Cai et al., 2015); (C) Jingyuan magnetic susceptibility (orange) (Sun et al., 2006); (D) Dongge cave $\delta^{18}O$ (dark blue) (Kelly et al., 2006); (E) Sanbao $\delta^{18}O$ (magenta) (Wang et al., 2008); (F) Kesang $\delta^{18}O$ (green) (Cheng et al., 2012); (G) Tianmen $\delta^{18}O$ (red) (Cai et al., 2010). Stronger/weaker monsoons indicated by proxies during MIS-5c and MIS-5e are marked by 'S'/'W', respectively. (H) July insolation (blue) at 65°N (Berger, 1978). (For interpretation of the references to color in this figure legend, the reader is referred to the web version of this article.)

inconsistency are as follows: (1) the $\delta^{18}O$ is completely not a proxy of Asian monsoon intensity although the caves are located in the monsoon areas; (2) The $\delta^{18}O$ can represent the variation of Asian monsoon but in different regions their amplitudes are not in agreement. In addition, the explanation of cave $\delta^{18}O$ may depend on different timescale. For example, results from an isotope-enabled climate model indicated that the Asian speleothem $\delta^{18}O$ are not a valid proxy for monsoon intensity only on the astronomical timescale (Caley et al., 2014).

If we suppose that the cave $\delta^{18}O$ reflects the intensity of Asian monsoon as some of the studies said (e.g., Wang et al., 2008; Cai et al., 2015; Cheng et al., 2016), it reveals that $\delta^{18}O$ records have regional differences. Over the typical East Asian monsoon region, the Sanbao record indicates that the $\delta^{18}O$ value is less negative in MIS-5e than in MIS-5c (Fig. 1); however, over the southwestern China and southern Tibetan Plateau influenced more by the Indian monsoon, the $\delta^{18}O$ values in Xiaobailong, Dongge and Tianmen caves are more negative in MIS-5e (Kelly et al., 2006; Cai et al., 2010, 2015). These features imply that the East Asian and Indian monsoons may exert distinct responses to the insolation changes. Furthermore, the "less negative $\delta^{18}O$-weaker monsoon" relationship widely used in stalagmite studies results in an inconsistency between cave and loess records over East Asian monsoon area that the stronger monsoon occurs in MIS-5e for loess and in MIS-5c for stalagmites.

In order to clarify the regional disagreements among proxies, a set of numerical simulations are held in this study to examine the sensitivity of the Asian monsoon system to different insolation forcing. Using a coupled ocean-atmosphere model, the responses of Asian monsoon during MIS-5c and MIS-5e are simulated under prescribed astronomical configurations, respectively. The model and experiments are described in Section 2 and the results are analyzed and discussed in Sections 3 and 4, respectively. Major points are concluded in the final section.

2. Numerical experiments

The climate model used in this study is the National Center for Atmospheric Research's (NCAR's) Community Climate System Model version 3 (CCSM3) (Collins et al., 2006). CCSM3 is a coupled atmosphere-ocean-land-sea ice model in which the atmospheric module is the Community Atmosphere Model (CAM); they have been widely used to simulate the past climate change over Asia (e.g., Otto-Bliesner et al., 2006; Liu et al., 2014). Three experiments (namely, PI, MIS-5c, MIS-5e) are carried out to simulate the Asian monsoon climatology during the preindustrial, MIS-5c and MIS-5e, respectively. To test the sensitivity of climate model to the astronomical insolation, the climatic forcings we included here are only the changes in astronomical parameters. The prescribed astronomical configurations for PI, MIS-5c (100.3 kyr B.P.) and MIS-5e (130.7 kyr B.P.) are shown in Table 1. The atmospheric greenhouse gas concentrations are set to pre-industrial values and other boundary conditions (e.g., vegetation, ice sheet cover) are kept as present. Since the ice sheets over the Northern Hemisphere are limited, our experiments should capture the first-order response of Asian monsoon during interglacials. The horizontal resolution for atmosphere is set to T42, approximately corresponding to 2.8° × 2.8°. Each experiment is integrated for 435 years and the results for the last 35 years are averaged and analyzed.

In boreal summer, the simulated 850 hPa wind vectors in the PI experiment show a similar circulation pattern as observed over the Asian monsoon areas (not shown). The southwesterly winds pass over the Arabian Sea and convert to be westerly winds when reach Indian subcontinent. Over East Asia, the monsoon is characterized by strong southerly winds over continents. The simulated distributions of precipitation rates are also in qualitative agreement with observations. Of note is that it is difficult for the deep oceans to reach equilibrium in 400-year integrations and the potential feedbacks from deep oceans might be neglected. However, since the focused Asian monsoon is more likely a response of atmosphere-surface ocean system, it is still reasonable to examine the primary changes in Asian monsoon in these experiments.

3. Results

Compared to the preindustrial at astronomical-induced insolation minimum, the MIS-5c and MIS-5e insolation in averaged boreal summer

Table 1
Orbital parameters used in the experiments.

Experiment ID	Longitude of perihelion	Obliquity	Eccentricity
PI	102.72	23.44	0.0167
MIS-5c	277.33	22.96	0.0402
MIS-5e	259.70	24.13	0.0390

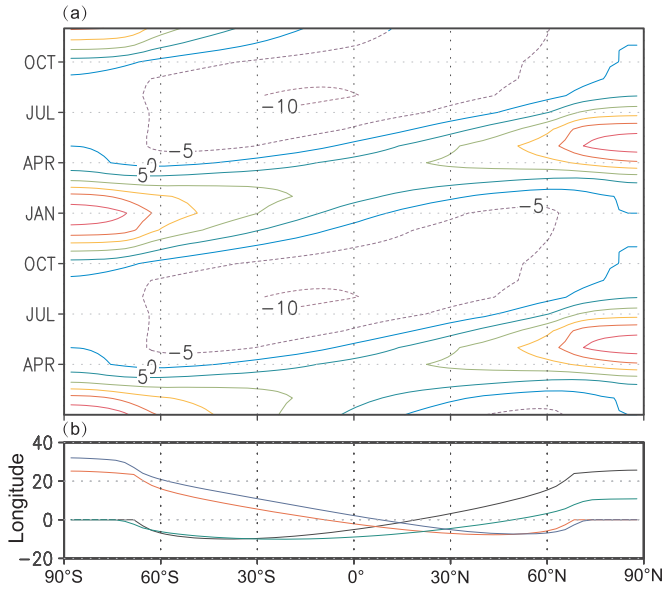

Fig. 2. (A) Time-latitude section of insolation difference (W/m^2) between MIS-5e and MIS-5c in our experiments; (B) Insolation difference (W/m^2) in April (red), May (dark blue), June (black), July (green) and August (light blue). (For interpretation of the references to color in this figure legend, the reader is referred to the web version of this article.)

are both larger over the Northern Hemisphere. For the differences in the insolation between MIS-5e and MIS-5c (Fig. 2A), it can be shown that not the insolation values of each summer month and of each latitude are larger in MIS-5e than those in MIS-5c over the latitudes as the traditional Milankovitch forcing at 65°N (Fig. 1). In contrary, the boreal summer insolation decreases by a range of approximately 0–10 W/m^2 over the tropics and southern hemisphere. This decreased insolation starts at the southern areas in boreal spring and extends northward. In fall, it reaches the peak and is negative over nearly all the latitudes.

To see the insolation difference of the specific month, we choose the April, May, June, July and August insolation here (Fig. 2B). In April and May, the northern insolation in MIS-5e is totally larger than that in MIS-5c. In June (approximately at solstices), the zero-difference point is approximately at 15°N and the insolation differences between MIS-5e and MIS-5c are positive over the extratropical regions. Then the northern insolation differences decrease with latitudes in July and the zero-difference point moves northward to about 45°N. In August, only the differences over some of the polar region are positive. Distinct differences between low- and high-latitude insolation over the Northern Hemisphere might lead to a complicated response of Asian summer monsoon. Thus, we cannot simply choose the high-latitude insolation as a reference curve considering that the Asian monsoon is a tropical/subtropical climate system.

Under the change in insolation distributions, the low-level air temperature in boreal summer does not respond longitude-consistently as the forcing, primarily due to the land-sea configuration (Fig. 3). Compared to the PI experiment, the 850 hPa air temperature during MIS-5c and MIS-5e is both higher over mid- to high-latitudes over northern hemisphere in boreal summer, with larger differences over the continents than over the oceans (Fig. 3A, B). Over the low latitudes, the warming is not so significant and in some regions a cooling is found. For the differences between MIS-5e and MIS-5c, the summer 850 hPa temperature is declined over the tropics (Fig. 3C) due to the weaker solar insolation in MIS-5e (Fig. 2). Except for the cooling centers of Arabian Peninsula-Sahara, the temperature decrease is not obvious because of the huge heat capacity of oceans. The most sensitive warming is located over the Eurasian and North American continent, with a warming of about 0.8 °C.

Compared to the PI experiment, the sea level pressure weakens over the mid-latitude continents while strengthens over the Pacific and Indian Oceans in the MIS-5c and MIS-5e experiments, which amplifies the pressure gradients between land and ocean over Asian monsoon areas in both stages (Fig. 4). Over East Asia, the amplified pressure gradients result in stronger monsoons in MIS-5c and MIS-5e, as the anomalous southerly winds and heavier precipitation indicate (Figs. 5A, B, 6A, B); these responses of monsoon are similar with that during mid-Holocene shown by the Paleoclimate Model Intercomparison Project (PMIP) results (Jiang et al., 2013). In the differences between MIS-5e and MIS-5c, the intensified subtropical high pressure cell over the northwestern Pacific, together with the intensified continental low pressure (Fig. 4C), facilitates for the development of an anticyclone anomaly (Fig. 5C). The anticyclone covers the southern Japan and spreads to the China continent, inducing southerly wind anomaly over eastern and northeastern China (Fig. 5C), which reinforces the East Asian monsoon and especially shifts it further northward. The changes in summer precipitation over East Asia exhibit a remarkable tripole pattern from the south to north although in some places the differences are not statistically significant (Fig. 6C). Over the middle regions controlled by the anomalous anticyclone, the vertical convection is suppressed; however, the summer precipitation in further north is obviously enlarged due to the increased frontal rainfall. Compared to the present-day, the sensitive response of rainfall is simulated over the further northern regions over the boreal insolation maxima (MIS-5c and MIS-5e). Thus, the variation of East Asian monsoon linearly follows the Milankovitch forcing at 65°N; the typical monsoon southerly wind is significantly stronger during MIS-5e than MIS-5c.

For the Indian monsoon, however, the situation is quite different. Compared to the PI experiment, the increased meridional pressure gradient between Indian Ocean and Eurasian continent (Fig. 4A, B) leads to northward movement of the monsoon in both MIS-5c and MIS-5e, which is characterized by the stronger northern branch and weaker southern branch (Fig. 5A, B). The circulation pattern allows the summer precipitation to increase in the north but to decrease in the south (Fig. 6A, B). For the MIS-5e minus MIS-5c, a key system for Indian monsoon change is the low pressure anomaly located over the Arabian Sea, although it is not statistically significant in the sea-level pressure changes (Fig. 4C). More solar heating over land and less over ocean amplify the meridional temperature gradient (Fig. 3C) and ought to intensify the cross-equatorial current and Indian monsoon circulation. But this impact is corrupted by this Arabian Sea cyclonic anomaly, as clearly seen in the wind vector changes (Fig. 5C). The 'canonial' strengthened westerly wind over India and Bay of Bengal disappears and turns northwestward (Fig. 5C). As a result, the monsoon wind does not significantly change after reaching the Indian continent (Fig. 5C). On the other hand, strong moisture convergence is induced and the rainfall is significantly promoted over the Arabia Sea, leaving the precipitation over downstream areas to change slightly (Fig. 6C). Hence, the response of the Indian monsoon is distinctly different from that of the East Asian monsoon from a seasonally averaged perspective. Due to the lower latitude location, the Indian monsoon is not significantly intensified in MIS-5e as its East Asian counterpart.

To examine the sensitivity of monsoon precipitation to the insolation changes, a simple linear relationship is assumed that the precipitation changes ΔP is proportional to the insolation changes ΔS, i.e., $\Delta P = \lambda \Delta S$ where λ is the sensitivity factor. Since the insolation differences between MIS5c and MIS5e is different over different latitudes, the λ can reflect the amplitude of the precipitation response to the same insolation change. The spatial pattern of λ_f, as defined by the following expression

$$\lambda_f = \frac{\lambda_{5e}}{\lambda_{5c}} = \frac{(P_{5e} - P_{PI}) \times (S_{5c} - S_{PI})}{(P_{5c} - P_{PI}) \times (S_{5e} - S_{PI})} \quad (1)$$

is shown in Fig. 7. Over the northern hemisphere, the largest response of summer precipitation is found over Korea, Japan and surrounding ocean, which corresponds to the negative precipitation

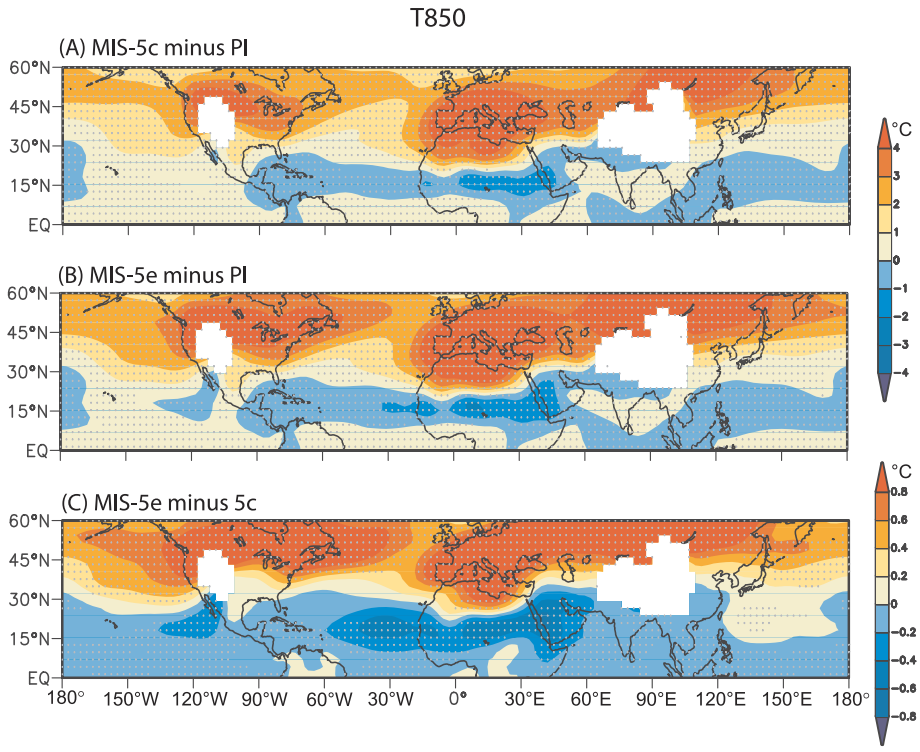

Fig. 3. Differences in the northern hemispheric 850 hPa temperature (°C) during boreal summer between the experiments MIS-5c and PI (A), MIS-5e and PI (B), as well as MIS-5e and MIS-5c (C). Grey dotted show the grids statistically significant at 95% confidence level.

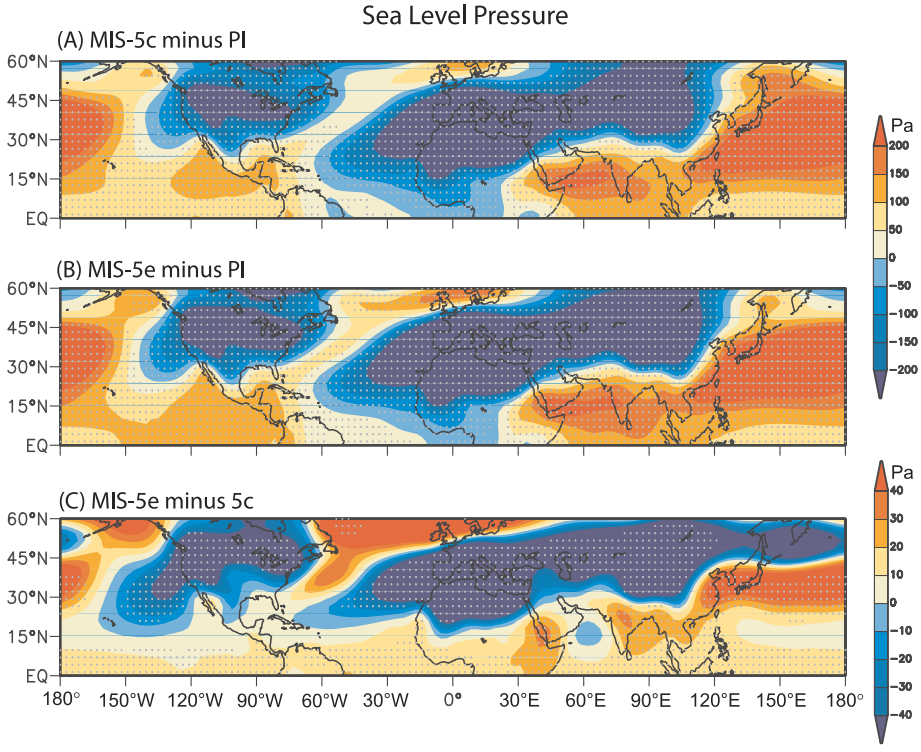

Fig. 4. Similar with Fig. 3, but for the differences in sea level pressure (Pa).

anomaly between MIS-5e and MIS-5c, indicating that the East Asian monsoon is most sensitive to the insolation change over this area. As the front shifts northwards to northeastern China in warmer stages, this area suffers a big loss of precipitation. The sensitivity over northeastern China is relatively weaker because the insolation differences at the same latitudes are larger. Compared to the East Asian monsoon, the precipitation over Indian monsoon and other tropical areas responds not so significantly.

Except for the mean climatology, the detailed developing processes of Asian monsoon are also examined since the insolation differences between MIS-5c and MIS-5e for each month during the monsoon period are remarkably distinct. The responses of Asian monsoon from the onset to the withdrawal (May to September, respectively) are shown in Figs. 8 and 9. In May, the northern hemispheric insolation is almost larger in MIS-5e, which leads to higher surface air temperature over the entire Asian continent except the India and Arabian Peninsula (Fig. 8A). In

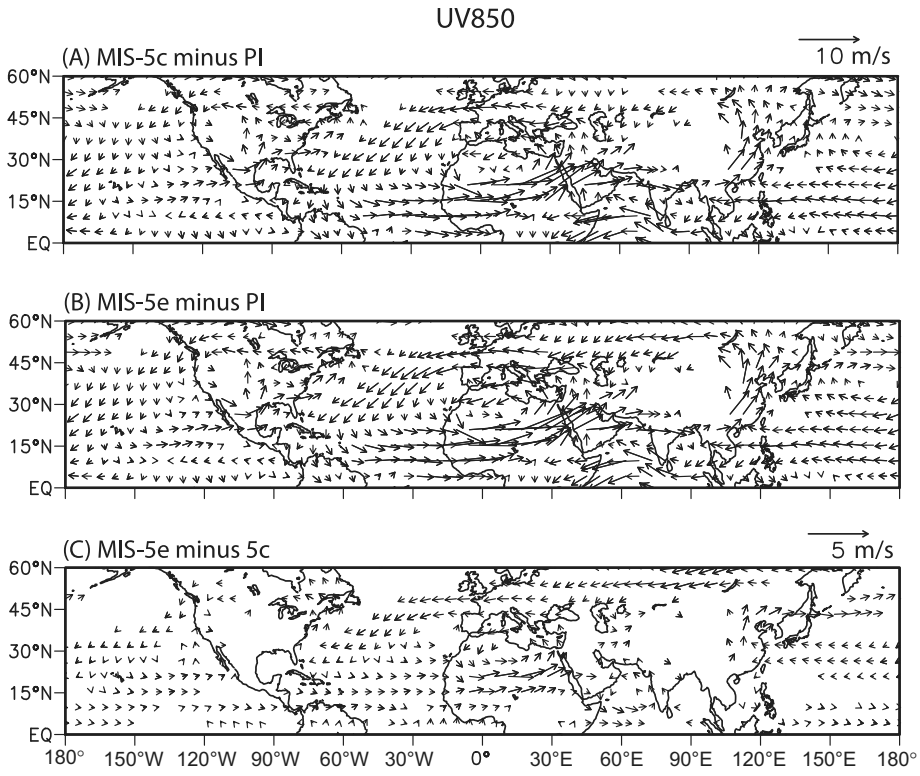

Fig. 5. Similar with Fig. 3, but for the differences in 850 hPa wind vectors (m/s). Only the differences statistically significant at 95% confidence level are shown.

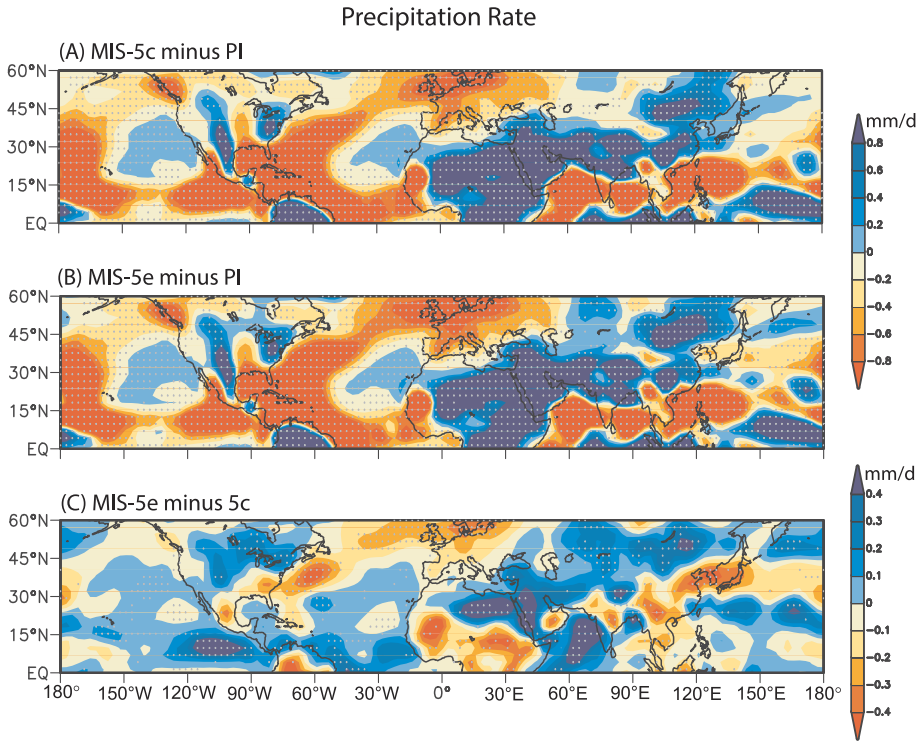

Fig. 6. Similar with Fig. 3, but for differences in the precipitation rates (mm/d).

June, the larger MIS-5e insolation shifts to the north of 15°N and the higher temperature over Asia also moves to the north of approximately 30°N (Fig. 8C). Afterwards, the MIS-5e warming continues to gradually retreat northwards in July, August and September (Figs. 8E, 9A, C), following the surface temperature changes.

The northward shift in the temperature gradients induces a similar trend of the response of monsoonal southerly winds over East Asia (Figs. 8, 9). In May, the intensified southerly winds in MIS-5e are found significant over the northern China covering 30°-40°N (Fig. 8B) and they extend to 45°N and 50°N in June and July, respectively (Fig. 8D, F). As the wind anomaly extends northwards, more water vapor is delivered to the north/northwest, which results in heavier precipitation over northeastern and central China. In contrast, the precipitation is reduced over southeastern China, the Yangtze and Yellow River valleys and the northern China in May, June and July, respectively, which is consistent with the northward shift of monsoon anomaly. In August and

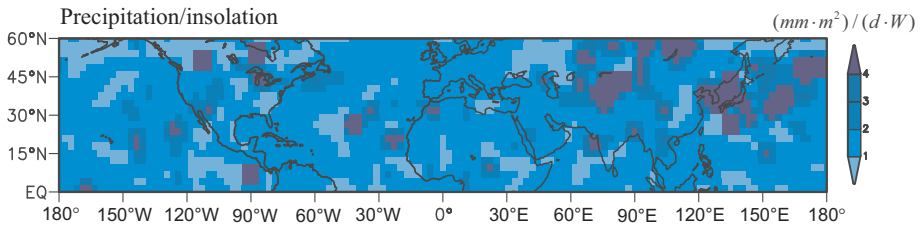

Fig. 7. Spatial pattern for the sensitivity factors of boreal summer precipitation rates versus the insolation change. See the text for the definition of sensitivity factor.

September when the East Asian monsoon tends to withdraw, the monsoon winds do not vary obviously and the precipitation is suppressed but not statistically significant over eastern China (Fig. 9B, D). An anomalous cyclone is produced over the Far East, promoting the rainfall in this area.

The domains of Asian summer monsoon are also calculated based on the definition of Wang et al., (2012). Model grids, which the summer-minus-winter precipitation rate exceed 2.0 mm/d and the summer precipitation exceed 55% of the annual total amount, are considered as the monsoon area. The boreal summer refers to May, June, July August and September and the winter refers to November, December, January, February and March. The domains of Asian summer monsoon in three experiments generally cover across the Arabian Sea, Indian subcontinent, the Bay of Bengal, Indochina peninsula and the eastern and northeastern China (Fig. 10). Compared to PI, the domains of Indian monsoon do not remarkably vary in MIS-5c and MIS-5e and only a few grids is increased in the northern area and decreased in the southern area (Fig. 10A–C). In contrast, the East Asian monsoon grids over northern China expand significantly to the north and northwest by about 18 grids from the MIS-5c to the PI experiments (Fig. 10A, B). Further, the East Asian monsoon area continues to spread northwards and northwestwards by about 13 grids in MIS-5e (Fig. 10C). Thus, the domain of East Asian monsoon is more sensitive to the insolation forcing than the Indian monsoon, in agreement with their intensity.

On the African sector, the strong extratropical warming (Fig. 3C) produces another anomalous low pressure over northern Africa (Fig. 4C) besides the Arabian Sea cyclone. These two systems act to intensify the westerly wind and allow the Atlantic moisture to penetrate farther inland (Fig. 5C). Thus, an obvious precipitation increase occurs in the eastern Sahara (Fig. 6C); however, the rainfall is suppressed over the western African monsoon regions due to the lack of atmospheric water vapor (Fig. 6C). This simulated sensitive rainfall variation over Africa to the astronomical change is similar with those found in previous studies (Claussen et al., 1999; Liu et al., 2003).

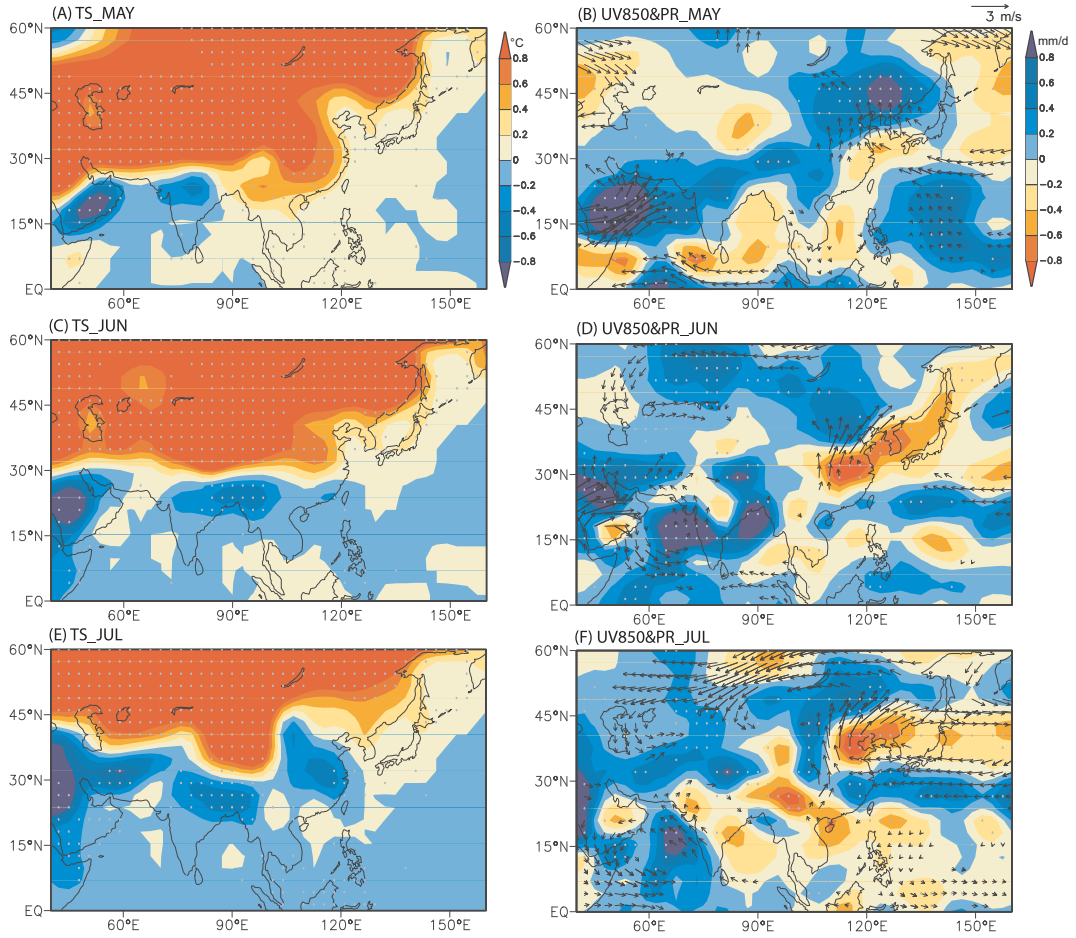

Fig. 8. Differences in the surface temperature (°C, left column), 850 hPa wind vectors (m/s, right column) and precipitation rates (mm/d, shaded) in May (A, B), June (C, D) and July (E, F). Grey dotted are the differences in temperature and precipitation rates statistically significant at 95% confidence level, respectively. Only the differences in wind vectors statistically significant at 95% confidence level are shown.

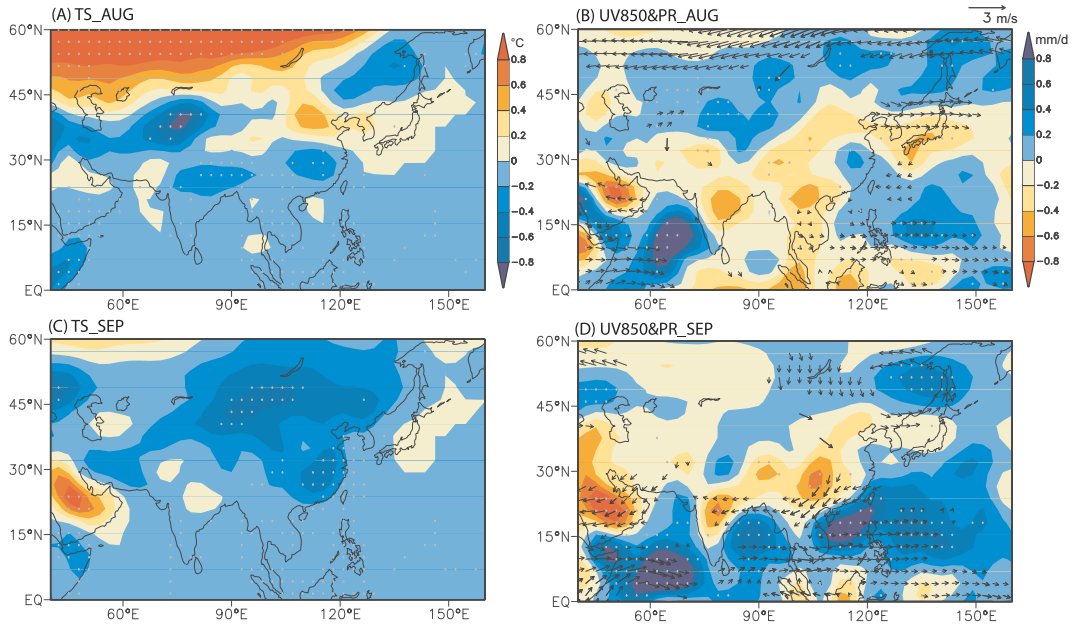

Fig. 9. Similar with Fig. 8, but for August and September.

4. Discussion

Although the monsoon is a complex system with the wind reversal and plentiful rainfall included, most of the proxies of East Asian monsoon are related to the precipitation in paleoclimate reconstructions. However, not all the precipitation changes over East Asia follow the monsoon response to the astronomical forcing. Similar with those on the interannual timescale, the response of precipitation to astronomical forcing over the northern rain belt is more consistent with the wind intensity because stronger East Asian monsoon usually moves further northward, while the southern rainfall is out of phase probably due to an ENSO modulation (Shi et al., 2012). Particularly in the optimal climatic period MIS-5e, the simulated increase in precipitation is consistent with the larger magnetic susceptibility in loess (Sun et al., 2006, 2015) and this increase is found most sensitive at approximately 50°N with the northward jump of East Asian rain belt. Although the sensitive areas might depend on the performance of our model, it is still highlighted that the rainfall over northern monsoon edges responds significantly to the insolation changes. The grain size data shows an advance of rain belt during the MIS5 (Yang and Ding, 2008), which is actually qualitatively consistent with our simulated heavier rainfall. This coincidence between northern precipitation and East Asian monsoon intensity is also found since the last glacial maximum (Liu et al., 2014). Hence, the Chinese loess at northern regions does not merely

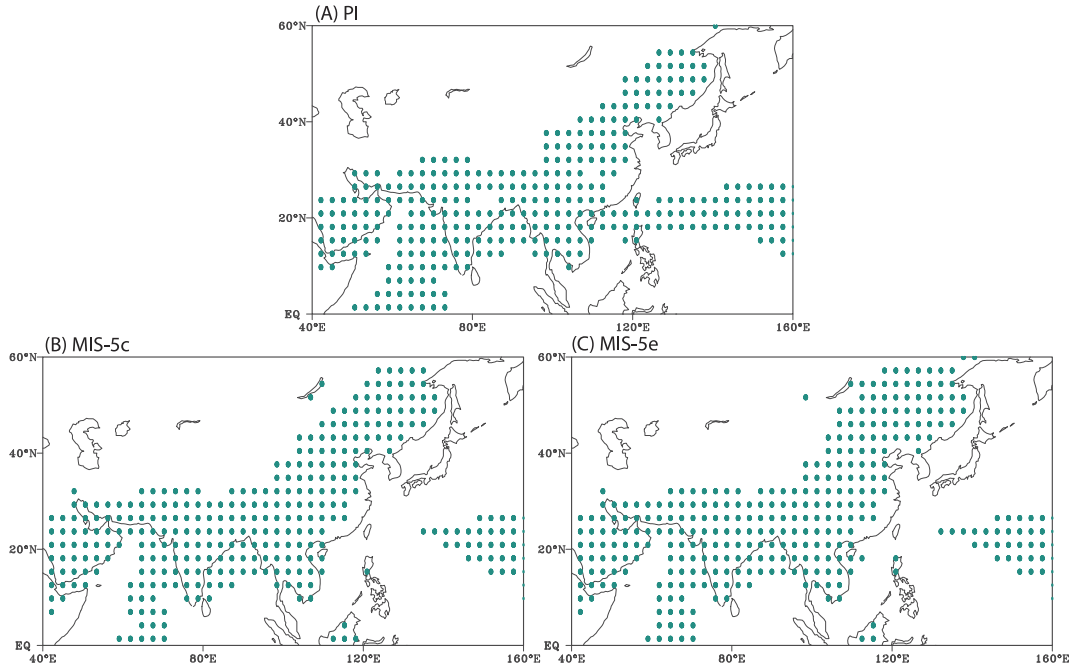

Fig. 10. Domains of the Asian summer monsoon as defined by the local summer (here refers to May, June, July August and September)-minus-winter (here refers to November, December, January, February and March) precipitation rate exceeding 2.0 mm/d and the local summer precipitation exceeding 55% of the annual total for the experiments (A) PI, (B) MIS-5c and (C) MIS-5e.

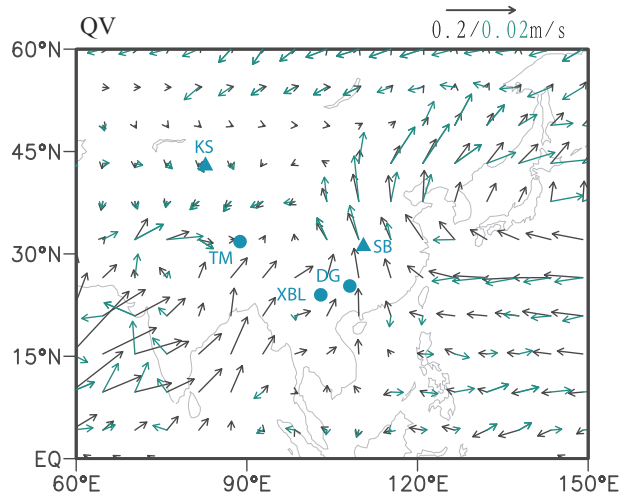

Fig. 11. Differences in the surface water vapor flux ($kg{\cdot}m{\cdot}kg^{-1}\,s^{-1}$) between MIS-5e and MIS-5c (green vectors). Only the flux differences statistically significant at 95% confidence level are shown. For reference, the surface water vapor flux in MIS-5e is also shown as black vectors. The scales for the black and green vectors are shown in the same colors on the top right, respectively. Locations of stalagmite records are also marked as dots (KS: Kesang, TM: Tianmen, XBL: Xiaobailong, DG: Dongge, SB: Sanbao). (For interpretation of the references to color in this figure legend, the reader is referred to the web version of this article.)

record the local precipitation changes but also are good indicators of East Asian monsoon intensity at least for the warm periods.

To explain the differences in stalagmite $\delta^{18}O$ records on relative intensity between MIS-5c and MIS-5e (Fig. 1), the responses of water vapor fluxes over Asia are further examined (Fig. 11). Basically, the water vapor over Asian continent in boreal summer is primarily originated from Indian and Pacific Oceans, which is delivered by Indian and East Asian summer monsoon (Fig. 11). For the precipitation $\delta^{18}O$ at Chinese caves, it would be more negative if the water vapor comes from Indian Ocean, compared to that from Pacific. The water vapor from Indian Ocean is carried by the cross-equatorial air stream and reaches the continent after a huge loss by raining-out over India and Bay of Bengal. During this remote journey to the Chinese continent, the fractionation process which the water vapor undergoes is significant and results in a more negative $\delta^{18}O$ value at the destination. However, for the water vapor from Pacific, the rain-out effect is relatively weak due to short distance for transportation and the precipitation $\delta^{18}O$ value is less negative. Compared to MIS-5c, the water vapor flux from Pacific Ocean is significantly increased during MIS-5e (Fig. 11), which promotes its relative contribution in the $\delta^{18}O$ changes for the downstream caves; this might be the reason why we observed in Sanbao and Kesang caves that the MIS-5e $\delta^{18}O$ value is less negative than the MIS-5c (Fig. 1). Thus, less negative values in the cave records actually reflect more moisture transport from Pacific in MIS-5e, which imply a stronger East Asian monsoon circulation. From the minimal to maximal insolation, more negative $\delta^{18}O$ represents stronger circulation but during different maximal insolation, more negative $\delta^{18}O$ might be not equal to stronger circulation. In contrast, the Tianmen, Dongge and Xiaobailong caves are all located at the regions where the water vapor flux is simulated from Indian Ocean, although in most Indian monsoon regions the flux change is not statistically significant (Fig. 11). From this perspective, the stalagmite $\delta^{18}O$ is more likely an indicator of water vapor transportation associated with the large-scale circulation but cannot linearly reflect the Asian monsoon intensity (e.g., the precipitation), at least for the astronomical timescale; this implication supports the conceptual explanation for the stalagmite $\delta^{18}O$ changes from a perspective of circulation effect (Tan, 2013; Caley et al., 2014; Rao et al., 2014). Furthermore, the monsoon intensity during the Holocene, as recorded by the traditional monsoon proxy of moisture or precipitation records from northern China, is obviously different from the stalagmite $\delta^{18}O$ records (Liu et al., 2015, 2017), which also implies that the explanation on the stalagmite $\delta^{18}O$ is more complicated.

Although our results reveal the complexity of Asian monsoon precipitation responding to the astronomical change, they are still ideal since only the solar forcing is considered in the experiments. Even both at precession minima of the last interglacial, the limited volumes of global ice sheets at MIS-5c and MIS-5e are still not the same, with the latter a little smaller (Lisiecki and Raymo, 2005). The influences from the ice sheets certainly exist and make the response of Asian monsoon more complex. The difference in East Asian monsoon might be amplified since deposit records always indicate that the northern ice sheets exert a reverse effect on the monsoon intensity (Morley and Heusser, 1997; An et al., 2011), however, it is still questionable whether and how the ice sheets affect the tropical/subtropical monsoons (Clemens and Prell, 2003; Yin et al., 2009). Duration effect of the rainy season, which is found significant over northern China (Shi, 2016), may also play a role in the response of Asian monsoon precipitation, although it might be not obvious in differences between two precession minima in this study.

5. Conclusions

Under the different astronomical configurations, model experiments held in this study indicate complicated, not simply linear, responses of Asian monsoon intensities in MIS-5c and MIS-5e. The Asian monsoon responses vary with regions and signals. Inconsistency in the heating differences over tropics and high-latitudes might lead to diverse monsoon changes. The East Asian monsoon is significantly intensified in MIS-5e due to an anomalous anticyclone over northwestern Pacific and shifts the rain-belt to further north. For the Indian monsoon, the upward motion by the warming over Arabian Sea blocks the strong moisture transportation from southern ocean and facilitates for the local precipitation, but the monsoon westerly over India and Bay of Bengal does not significantly vary. Distinct changes in the Indian and East Asian monsoon circulations modulate the relative contributions of Indian and Pacific Oceans on water vapor $\delta^{18}O$, thus providing an explanation for the regional differences among stalagmites. Although the stalagmite $\delta^{18}O$ variations in southern China are closely linked to the large-scale monsoon circulation, it is still difficult to expect them to linearly reflect the monsoon intensity. Anyhow, the responses of Asian monsoon to the insolation forcing are more complicated than traditionally expected and are still required to be further explored.

Acknowledgments

The authors thank two reviewers for their valuable comments, which are useful to revise the manuscript. We also thank Drs. Youbin Sun, Long Ma, Xingxing Liu for their discussion on the geological proxies. This work is jointly supported by the National Natural Science Foundation of China (41690115, 41572160), the National Key Research and Development Program of China (2016YFE0109500), and the Chinese Academy of Sciences (QYZDY-SSW-DQC001 and ZDBS-SSW-DQC001) and the Youth Innovation Promotion Association CAS.

References

An, Z.S., Kukla, G., Porter, S.C., Xiao, J.L., 1991. Magnetic susceptibility evidence of monsoon variation on the Loess Plateau of Central China during the last 130,000 years. Quat. Res. 36, 29–36.

An, Z.S., et al., 2011. Glacial-interglacial Indian summer monsoon dynamics. Science 333, 719–723.

Berger, A.L., 1978. Long-term variations of caloric insolation resulting from the Earth's orbital elements. Quat. Res. 9, 139–167.

Cai, Y.J., Cheng, H., An, Z.S., Edwards, R.L., Wang, X.F., Tan, L.C., Wang, J., 2010. Large variations of oxygen isotopes in precipitation over south-central Tibet during Marine Isotope Stage 5. Geology 38, 243–246.

Cai, Y.J., Fung, I.Y., Edwards, R.L., An, Z.S., Cheng, H., Lee, J.E., Tan, L.C., Shen, C.C.,

Wang, X.F., Day, J.A., Zhou, W.J., Kelly, M.J., Chiang, J.C.H., 2015. Variability of stalagmite-inferred Indian monsoon precipitation over the past 252,000 y. In: Proceedings of the National Academy of Sciences. 112. pp. 2954–2959.
Caley, T., Roche, D.M., Renssen, H., 2014. Orbital Asian summer monsoon dynamics revealed using an isotope-enabled global climate model. Nat. Commun. 5, 5371. http://dx.doi.org/10.1038/ncomms6371.
Cheng, H., Zhang, P.Z., Spotl, R.L., Edwards, R.L., Cai, Y.J., Zhang, D.Z., Sang, W.C., Tan, M., An, Z.S., 2012. The climatic cyclicity in semiarid-arid central Asia over the past 500,000 years. Geophys. Res. Lett. 39, L01705. http://dx.doi.org/10.1029/2011GL050202.
Cheng, H., Edwards, R.L., Sinha, A., SpÖtl, C., Yi, L., Chen, S., Kelly, M., Kathayat, G., Wang, X., Li, X., Kong, X., Wang, Y., Ning, Y., Zhang, H., 2016. The Asian monsoon over the past 640,000 years and ice age terminations. Nature 534, 640–648.
Claussen, M., Kubatzki, C., Brovkin, V., Ganopolski, A., Hoelzmann, P., Pachur, H., 1999. Simulation of an abrupt change in Saharan vegetation in the mid-Holocene. Geophys. Res. Lett. 26, 2037–2040.
Clemens, S.C., Prell, W.L., 2003. A 350,000 year summer-monsoon multi-proxy stack from the Owen Ridge, northern Arabian Sea. Mar. Geol. 201, 35–51.
Clemens, S.C., Prell, W.L., Sun, Y.B., 2010. Orbital-scale timing and mechanisms driving late Pleistocene Indo-Asian summer monsoons: reinterpreting cave speleothem $\delta^{18}O$. Paleoceanography 25, PA4207. http://dx.doi.org/10.1029/2010PA001926.
Collins, W.D., et al., 2006. The Community Climate System Model version 3 (CCSM3). J. Clim. 19, 2122–2143.
Jiang, D.B., Lang, X.M., Tian, Z.P., Ju, L.X., 2013. Mid-Holocene East Asian summer monsoon strengthening: insights from Paleoclimate Modeling Intercomparison Project (PMIP) simulations. Palaeogeogr. Palaeoclimatol. Palaeoecol. 369, 422–429.
Kelly, M.J., Edwards, R.L., Cheng, H., Yuan, D.X., Cai, Y.J., Zhang, M.L., Lin, Y.S., An, Z.S., 2006. High resolution characterization of the Asian monsoon between 146,000 and 99,000 years B.P. from Dongge Cave, China and global correlation of events surrounding Termination II. Palaeogeogr. Palaeoclimatol. Palaeoecol. 236, 20–38.
Kutzbach, J.E., 1981. Monsoon climate of the early Holocene: climate experiment with Earth's orbital parameter for 9000 years ago. Science 214, 59–61.
Kutzbach, J.E., Liu, X., Liu, Z., Chen, G., 2008. Simulation of the evolutionary response of global summer monsoons to orbital forcing over the past 280,000 years. Clim. Dyn. 30, 567–579.
Li, X., Liu, X., Qiu, L., An, Z., Yin, Z., 2013. Transient simulation of orbital-scale precipitation variation in monsoonal East Asia and arid central Asia during the last 150 ka. J. Geophys. Res. 118, 7481–7488.
Lisiecki, L., Raymo, M., 2005. A Pliocene-Pleistocene stack of 57 globally distributed benthic $\delta^{18}O$ records. Paleoceanography 20, PA1003. http://dx.doi.org/10.1029/2004PA001071.
Liu, X.D., Shi, Z.G., 2009. Effect of precession on the Asian summer monsoon evolution: a systematic review. Chin. Sci. Bull. 54, 3720–3730.
Liu, Z., Otto-Bliesner, B., Kutzbach, J., Li, L., Shields, C., 2003. Coupled climate simulation of the evolution of global monsoons in the Holocene. J. Clim. 16, 2472–2490.
Liu, Z., et al., 2014. Chinese cave records and the East Asia summer monsoon. Quat. Sci. Rev. 83, 115–128.
Liu, J.B., Chen, J.H., Zhang, X.J., Li, Y., Rao, Z.G., Chen, F.H., 2015. Holocene East Asian summer monsoon records in northern China and their inconsistency with Chinese stalagmite $\delta^{18}O$ records. Earth Sci. Rev. 148, 194–208.
Liu, J.B., Chen, S.Q., Chen, J.H., Zhang, Z.P., Chen, F.H., 2017. Chinese cave $\delta^{18}O$ records do not represent northern East Asian summer monsoon rainfall. Proc. Natl. Acad. Sci. U. S. A. http://dx.doi.org/10.1073/pnas.1703471114.
Morley, J., Heusser, L., 1997. Role of orbital forcing in east Asian monsoon climates during the last 350 kyr: evidence from terrestrial and marine climate proxies from core RC14-99. Paleoceanography 12, 483–493.
Otto-Bliesner, B.L., Brady, E.C., Clauzet, G., Tomas, R., Levis, S., Kothavala, Z., 2006. Last Glacial Maximum and Holocene climate in CCSM3. J. Clim. 19, 2526–2544.
Pausata, F., Battisti, D.S., Nisancioglu, K.H., Bitz, C.M., 2011. Chinese stalagmite $\delta^{18}O$ controlled by changes in the Indian monsoon during a simulated Heinrich event. Nat. Geosci. 4, 474–480.
Rao, Z.G., Liu, X.K., Hua, H., Gao, Y., Chen, F., 2014. Evolving history of the East Asian summer monsoon intensity during the MIS5: inconsistent records from Chinese stalagmites and loess deposits. Environ. Earth Sci. http://dx.doi.org/10.1007/s12665-014-3681-z.
Rao, Z.G., Li, Y.X., Zhang, J.W., Jia, G.D., Chen, F.H., 2016. Investigating the long-term palaeoclimatic controls on the δD and $\delta^{18}O$ of precipitation during the Holocene in the Indian and east Asian monsoonal regions. Earth Sci. Rev. 159, 292–305.
Shi, Z.G., 2016. Response of Asian summer monsoon duration to orbital forcing under glacial and interglacial conditions: implication for precipitation variability in geological records. Quat. Sci. Rev. 139, 30–42.
Shi, Z.G., Liu, X.D., Sun, Y.B., An, Z.S., Liu, Z., Kutzbach, J., 2011. Distinct responses of East Asian summer and winter monsoons to astronomical forcing. Clim. Past 7, 1363–1370.
Shi, Z.G., Liu, X.D., Cheng, X.X., 2012. Anti-phased response of northern and southern East Asian summer precipitation to ENSO modulation of orbital forcing. Quat. Sci. Rev. 40, 30–38.
Sun, Y.B., Chen, J., Clemens, S.C., Liu, Q.S., Ji, J.F., Tada, R., 2006. East Asian monsoon variability over the last seven glacial cycles recorded by a loess sequence from the northwestern Chinese Loess Plateau. Geochem. Geophys. Geosyst. 7, Q12Q02. http://dx.doi.org/10.1029/2006GC001287.
Sun, Y.B., Kutzbach, J., An, Z.S., Clemens, S., Liu, Z.Y., Liu, W.G., Liu, X.D., Shi, Z.G., Zheng, W.P., Liang, L.J., Yan, Y., Li, Y., 2015. Astronomical and glacial forcing of East Asian summer monsoon variability. Quat. Sci. Rev. 115, 132–142.
Tan, M., 2013. Circulation effect: response of precipitation $\delta^{18}O$ to the ENSO cycle in monsoon regions of China. Clim. Dyn. 42, 1067–1077.
Wang, Y.J., Cheng, H., Edwards, R.L., Kong, X.G., Shao, X.H., Chen, S.T., Wu, J.Y., Jiang, X.Y., Wang, X.F., An, Z.S., 2008. Millennial- and orbital-scale changes in the East Asian monsoon over the past 224,000 years. Nature 451, 1090–1093.
Wang, B., Liu, J., Kim, H., Webster, P.J., Yim, S., 2012. Recent change of global monsoon precipitation (1979-2008). Clim. Dyn. 39, 1123–1135.
Yang, S.L., Ding, Z.L., 2008. Advance–retreat history of the East-Asian summer monsoon rainfall belt over northern China during the last two glacial–interglacial cycles. Earth Planet. Sci. Lett. 274, 499–510.
Yin, Q.Z., Berger, A., Crucifix, M., 2009. Individual and combined effects of ice sheets and precession on MIS-13 climate. Clim. Past 5, 229–243.
Yin, Q.Z., Singh, U.K., Berger, A., Guo, Z.T., Crucifix, M., 2014. Relative impact of insolation and the Indo-Pacific warm pool surface temperature on the East Asia summer monsoon during the MIS-13 interglacial. Clim. Past 10, 1645–1657.